Acta Cryst E CRYSTALLOGRAPHIC COMMUNICATIONS

ISSN 2056-9890

Structure of metaraminol hydrogen tartrate from synchrotron X-ray data and density functional theory calculations

Jacob K. Salazar,[a] James A Kaduk,[b]* Anja Dosen[c] and Thomas N. Blanton[c]

[a]North Central College, Department of Chemistry, 131 S. Loomis St., Naperville IL 60540, USA, [b]North Central College, Department of Physics, 131 S Loomis St, Naperville IL 60540, USA, and [c]ICDD, 12 Campus Blvd., Newtown Square PA 19073-3273, USA. *Correspondence e-mail: kaduk@polycrystallography.com

Received 28 July 2026
Accepted 10 September 2026

Edited by W. T. A. Harrison, University of Aberdeen, United Kingdom

Keywords: powder diffraction; aramine; Rietveld refinement; density functional theory; crystal structure.

CCDC references: 2587069; 2587068

Supporting information: this article has supporting information at journals.iucr.org/e

The crystal structure of the title salt, $C_9H_{14}NO_2^+\cdot HC_4H_4O_6^-$, has been solved and refined using synchrotron X-ray powder diffraction data and optimized using density functional theory techniques. The crystal structure consists of alternating hydrophobic and hydrophilic layers lying parallel to the *ab* plane. Hydrogen bonds link the cations and anions in the hydrophilic layers. The anions are linked by very strong charge-assisted O—H···O hydrogen bonds into chains propagating along the *a*-axis direction. Each H atom of the protonated N atom of the cation acts as a donor in at least one N—H···O hydrogen bond to an anion.

1. Chemical context

Metaraminol hydrogen tartrate, $C_9H_{14}NO_2^+\cdot HC_4H_4O_6^-$ (**I**), also known as metaraminol bitartrate, and marketed as Aramine (obsolete), Pressonex and others in various countries, is used to treat hypotension (low blood pressure), particularly associated with patients receiving spinal anesthesia (Grauslyte *et al.*, 2022). The systematic name (CAS Registry Number 33402-03-8) is 3-[(1*R*,2*S*)-2-azaniumyl-1-hydroxypropyl]phenol (2*S*,3*S*)-hydrogen 2,3-dihydroxybutanedioate.

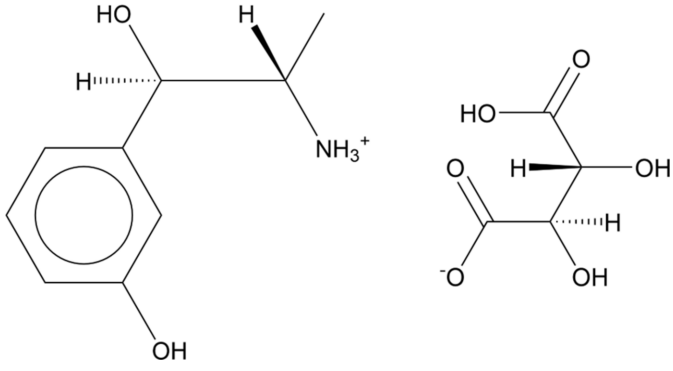

This work was carried out as part of a project (Kaduk *et al.*, 2014) to determine the crystal structures of large-volume commercial pharmaceuticals, and includes high-quality powder diffraction data for them in the Powder Diffraction File (Kabekkodu *et al.*, 2024).

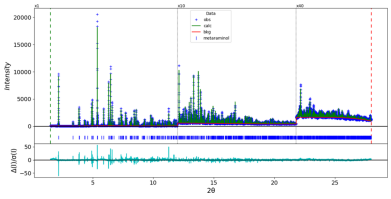

2. Structural commentary

The asymmetric unit of (**I**) is illustrated in Fig. 1 and consists of one $C_9H_{14}NO_2^+$ cation and one $HC_4H_4O_6^-$ anion in space

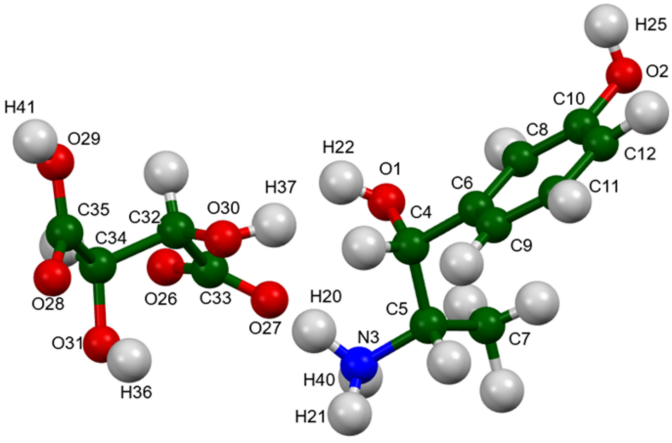

Figure 1
The asymmetric unit of (**I**), with the atom numbering. The atoms are represented by 50% probability spheroids.

group $P2_12_12_1$. The root-mean-square difference of the non-H atoms in the Rietveld-refined and *VASP*-optimized structures of (**I**), calculated using the *Mercury* (Macrae *et al.*, 2020) CSD-Materials/search/crystal packing similarity tool is 0.325 Å. The root-mean-square Cartesian displacements of the non-H atoms in the refined and optimized structures of the cation and anion, calculated using the *Mercury* calculate/molecule overlay tool, are 0.235 and 0.167 Å, respectively (Figs. 2 and 3). The agreements are within the normal range for correct structures (van de Streek & Neumann, 2014). The remaining discussion will emphasize the *VASP*-optimized structure.

Almost all of the bond distances, bond angles, and torsion angles fall within the normal ranges indicated by a *Mercury* Mogul geometry check (Macrae *et al.*, 2020). Only the C7—C5—C4 bond angle of 117.1° [average = 114.1 (9)°; *Z*-score = 3.4] is flagged as unusual. The standard uncertainty on the average is very small, inflating the *Z*-score, so this angle is not of concern. The conformation about the C6—C4—C5—N3 torsion angle is *trans* (179.2°), and falls within the normal distribution. The torsion angles involving rotation about the C4—C6 bond (such as 77.9° for C5—C4—C6—C8) fall within the typical broad ranges for similar torsion angles. The tartrate anion is in the *trans* conformation, as indicated by the C35—C34—C32—C33 torsion angle of −177.2°.

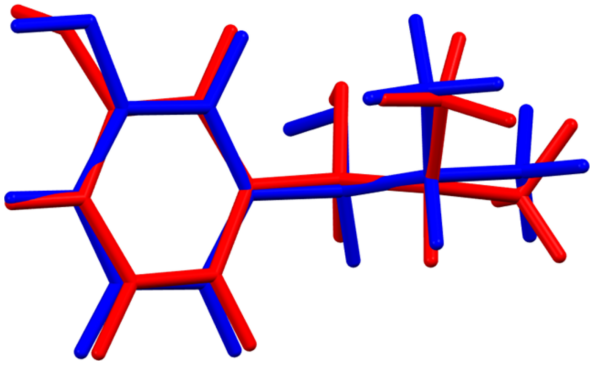

Figure 2
Comparison of the refined structure of the metaraminol cation in (**I**) (red) to the *VASP*-optimized structure (blue). The comparison was generated using the *Mercury* calculate/molecule overlay tool; the r.m.s. difference is 0.235 Å.

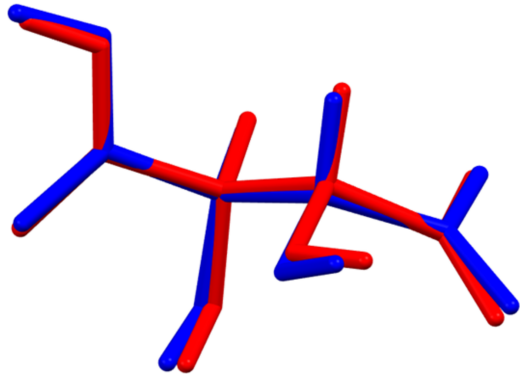

Figure 3
Comparison of the refined structure of the bitartrate anion in (**I**) (red) to the *VASP*-optimized structure (blue). The comparison was generated using the *Mercury* calculate/molecule overlay tool; the r.m.s. difference is 0.167 Å.

Quantum chemical geometry optimizations of the isolated metaraminol cation and bitartrate anion (DFT/B3LYP/6-31G*/water) using *Spartan '24* (Wavefunction, 2025) indicated that both the cation and anion were geometrically (r.m.s. difference = 0.277 and 0.173 Å, respectively) similar to local minima, but energetically different (6.1 and 21.2 kcal mol^{-1}, respectively). The global minimum-energy conformations were found to be more compact (featuring intramolecular hydrogen bonds), showing that intermolecular interactions are important in determining the solid-state conformations of these species in (**I**).

3. Supramolecular features

The extended structure of (**I**) (Fig. 4) consists of alternating hydrophobic and hydrophilic layers lying parallel to the *ab* plane. Hydrogen bonds (discussed below) link the cations and anions in the hydrophilic layers. The *Mercury* aromatics analyser indicated one strong (d = 4.97 Å) interaction between the phenyl rings of the cations, and two moderate (d = 6.15 Å)

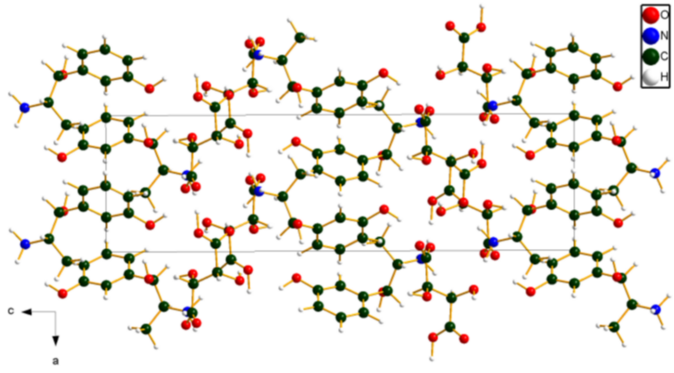

Figure 4
The crystal structure of (**I**), viewed down the *b*-axis direction.

Table 1
Hydrogen-bond geometry (Å, °).

D—H···A	D—H	H···A	D···A	D—H···A
O29—H41···O26^{i}	1.14	1.33	2.464	173
O30—H37···O1	0.99	1.70	2.686	169
O31—H36···O29^{ii}	0.99	1.95	2.885	156
O31—H36···O28	0.99	2.36	2.644	96
N3—H40···O31^{iii}	1.05	1.72	2.762	172
N3—H21···O28^{ii}	1.05	1.69	2.718	166
N3—H20···O27	1.05	1.78	2.796	161
N3—H20···O30	1.05	2.50	3.111	116
O2—H25···O27^{iv}	1.00	1.76	2.709	157
O1—H22···O2^{iv}	0.98	2.19	3.113	155
C5—H14···O26	1.10	2.40	3.364	145
C12—H24···O26	1.09	2.72	3.758	154
C4—H13···O28	1.11	2.61	3.410	128
C9—H19···O29	1.09	2.95	4.033	171

Symmetry codes: (i) $x-1, y, z$; (ii) $-x, y-\frac{1}{2}, -z+\frac{3}{2}$; (iii) $-x+1, y+\frac{1}{2}, -z+\frac{3}{2}$; (iv) $x-\frac{1}{2}, -y+\frac{3}{2}, -z+2$.

interactions. The mean plane of the phenyl ring in the asymmetric unit is approximately ($\bar{1}$11).

Analysis of the contributions to the total crystal energy of the structure using the Forcite module of *Materials Studio* (Dassault Systèmes, 2025) indicated that bond, angle, and torsion distortion terms contribute significantly to the intramolecular energy. The intermolecular energy is small, and is dominated by van der Waals attractions, which in this force field-based analysis includes hydrogen bonds. The hydrogen bonds are better discussed using the results of the DFT calculation.

Hydrogen bonds (Table 1) are prominent in the structure. The anions are linked by very strong charge-assisted O29—H41···O26 hydrogen bonds into chains propagating along the *a*-axis direction. The O29—H41 single bond has a Mulliken overlap population of 0.175 *e*, with a bond energy [calculated using the correlation of Rammohan & Kaduk (2018)] of 23.9 kcal mol^{-1}. The H41···O26 hydrogen bond is only slightly weaker, with an overlap population of 0.117 *e* and a bond energy of 18.7 kcal mol^{-1}. Both alcoholic hydroxyl groups of the hydrogen tartrate anion act as donors in O—H···O hydrogen bonds, one to another anion and one to a cation.

Each H atom of the protonated –N3H$_3^+$ grouping of the cation acts as a donor in at least one N—H···O hydrogen bond to an anion. The energies of these hydrogen bonds were calculated using the correlation of Wheatley & Kaduk (2019). One hydroxyl group of the cation forms an O—H···O hydrogen bond to another cation, while the other bonds to the anion. Several C—H···O hydrogen bonds (from both the cation and anion) also contribute to the cohesion of the structure.

The volume enclosed by the Hirshfeld surface of (**I**) (Fig. 5; Spackman *et al.*, 2021) is 366.73 Å^3, or 98.13% of 1/4 of the unit-cell volume. The packing density is thus typical. The close contacts (red in Fig. 5) correspond to the hydrogen bonds noted above. The volume per non-hydrogen atom is slightly smaller than normal, at 17.0 Å^3.

The Bravais–Friedel–Donnay–Harker (Bravais, 1866; Friedel, 1907; Donnay & Harker, 1937) algorithm suggests

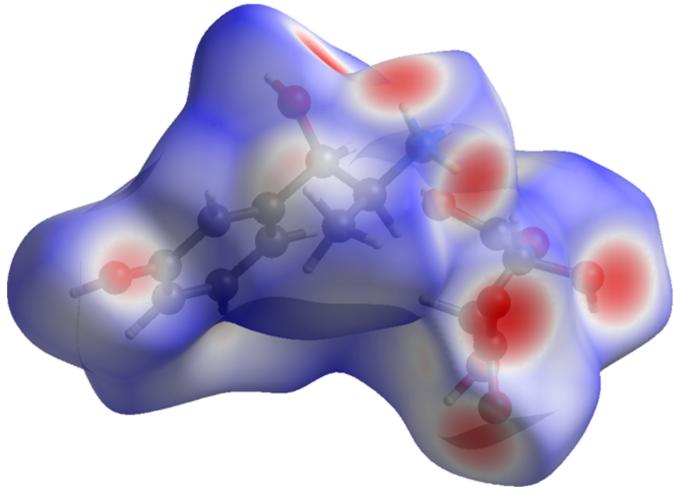

Figure 5
The Hirshfeld surface of (**I**). Intermolecular contacts longer than the sums of the van der Waals radii are colored blue, and contacts shorter than the sums of the radii are colored red. Contacts equal to the sums of radii are white.

that we might expect platy morphology for (**I**), with {001} as the principal faces. A second-order spherical harmonic model for preferred orientation was included. The texture index was 1.001, indicating that the preferred orientation was negligible in this rotated capillary specimen.

4. Database survey

A process for preparing metaraminol bitartrate is claimed in US Patent 10,087,136 B2 (Brenna *et al.*, 2018; Laboratori Alchemia S.r.l.), which includes NMR data, but no X-ray diffraction data, is provided. A synthesis method for metaraminol bitartrate is also claimed in Chinese Patent CN 103739504A (Pu *et al.*, 2013; Guangzhou Person Pharmaceutical Co., Ltd.). We are unaware of any published diffraction data for metaraminol bitartrate.

A reduced cell search in the Cambridge Structural Database (CSD version 2026.1.0; Groom *et al.*, 2016), combined with the chemistry C, H, N, and O only, yielded 31 hits, but no structures of metaraminol or its derivatives.

5. Synthesis and crystallization

Metaraminolhydrogen tartrate is a commercial reagent, purchased from TargetMol (Batch #118859), and was used as received.

6. Refinement

Crystal data, data collection and structure refinement details are summarized in Table 2. The white powder was packed into a 1.5 mm diameter Kapton capillary, and rotated during the measurement at ∼50 Hz. The powder pattern was measured at 295 K at beam line 11-BM (Lee *et al.*, 2008; Wang *et al.*, 2008; Antao *et al.*, 2008) of the Advanced Photon Source at

Table 2
Experimental details.

	(I)
Crystal data	
Chemical formula	$C_9H_{14}NO_2^+ \cdot C_4H_5O_6^-$
M_r	317.29
Crystal system, space group	Orthorhombic, $P2_12_12_1$
Temperature (K)	295
a, b, c (Å)	7.190512 (12), 8.421634 (17), 24.69323 (5)
V (Å^3)	1495.32 (1)
Z	4
Radiation type	Synchrotron, λ = 0.46873 Å
μ (mm^{-1})	0.001
Specimen shape, size (mm)	Cylinder, 2.0 × 1.5
Data collection	
Diffractometer	11-BM, APS
Specimen mounting	Kapton capillary
Data collection mode	Transmission
Scan method	Step
2θ values (°)	$2\theta_{min}$ = 0.510, $2\theta_{max}$ = 49.995, $2\theta_{step}$ = 0.001
Refinement	
R factors and goodness of fit	R_p = 0.090, R_{wp} = 0.105, R_{exp} = 0.039, $R(F^2)$ = 0.09024, χ^2 = 7.530
No. of parameters	85
No. of restraints	50
$(\Delta/\sigma)_{max}$	2.873

Computer programs: *GSAS-II* (Toby & Von Dreele, 2013) and *DIAMOND* (Crystal Impact, 2025).

Argonne National Laboratory using a wavelength of 0.4687342 Å from 0.5–50° 2θ with a step size of 0.001° and a counting time of 0.1 sec step^{-1}. The high-resolution powder diffraction data were collected using twelve silicon crystal analyzers that allow for high angular resolution, high precision, and accurate peak positions. A mixture of silicon (NIST SRM 640c) and alumina (NIST SRM 676a) standards (ratio Al_2O_3:Si = 2:1 by weight) was used to calibrate the instrument and refine the monochromatic wavelength used in the experiment.

The pattern was indexed on a primitive orthorhombic unit cell with a = 7.19584, b = 8.42890, c = 24.73316 Å, V = 1500.14 Å^3, and Z = 4 using *JADE Pro* (MDI, 2025). The suggested space group was $P2_12_12_1$, which was confirmed by the successful solution and refinement of the structure.

The molecular structure of metaraminol was downloaded from PubChem (Kim *et al.*, 2023) as Conformer3D_COMPOUND_CID_5906.sdf. It was converted to a *.mol2 file using *Mercury* (Macrae *et al.*, 2020), and to a Fenske–Hall Z-matrix using *Open Babel* (O'Boyle *et al.*, 2011). The tartrate anion model was taken from our structure of eliglustat hemitartrate (Kaduk *et al.*, 2026). The structure was solved using Monte Carlo simulated annealing techniques as implemented in *DASH* (David *et al.*, 2006), *EXPO2014* (Altomare *et al.*, 2013), and *FOX* (Favre-Nicolin & Černý, 2002). All three programs yielded essentially the same structure. The *EXPO2014* model was chosen for refinement.

Atom H40 was added to protonate N3 using *Materials Studio* (Dassault Systèmes, 2025). Analysis of O···O distances for potential hydrogen bonds suggested that O29 was protonated (O29···O26 = 2.39 Å), so H41 was added 0.90 Å from O29 on the O29···O26 vector using *Materials Studio*.

Rietveld refinement was carried out using *GSAS-II* (Toby & Von Dreele, 2013). Only the 1.5–28.0° portion of the pattern was included in the refinement (d_{min} = 0.969 Å). All non-H bond distances and angles were subjected to restraints, based on a *Mercury*/Mogul Geometry Check (Sykes *et al.*, 2011; Bruno *et al.*, 2004). The Mogul average and standard deviation for each quantity were used as the restraint parameters. The phenyl ring was restrained to be planar. The restraints contributed 1.5% to the overall χ^2. The hydrogen atoms were included in calculated positions, which were recalculated during the refinement using *Materials Studio* (Dassault Systèmes, 2025). The U_{iso} of the non-H atoms were grouped by chemical similarity. The U_{iso} of the H atoms were fixed at 1.2× the U_{iso} of the heavy atom to which they are attached. The peak profiles were described using a uniaxial microstrain model, with [001] as the unique axis. The background was modeled using a six-term shifted Chebyshev polynomial, with a peak at 6.00° to model the scattering from the Kapton capillary and any amorphous component of the sample.

The final refinement of 85 variables using 26,501 observations and 50 restraints yielded the residuals R_{wp} = 0.1055 and GOF = 2.74. The largest peak (0.24 Å from N3) and hole (0.82 Å from C6) in the difference Fourier map were calculated to be 0.56 (11) and −0.45 (11) e Å^{-3}, respectively. The final Rietveld plot is shown in Fig. 6. The largest features in the normalized error plot are in the shapes of some of the strong low-angle peaks.

The crystal structure of (**I**) was optimized (fixed experimental unit cell) with density functional theory techniques using *VASP* (Kresse & Furthmüller, 1996) through the *MedeA* graphical interface (Materials Design, 2024). The calculation was carried out on 32 cores of a 144-core (768 GB memory) HPE Superdome Flex 280 Linux server at North Central College. The calculation used the GGA-PBE functional, a plane wave cutoff energy of 400.0 eV, and a k-point spacing of 0.5 Å^{-1} leading to a 2 × 2 × 1 mesh, and took ∼8.5 h. Single-point density functional theory calculations (fixed experi-

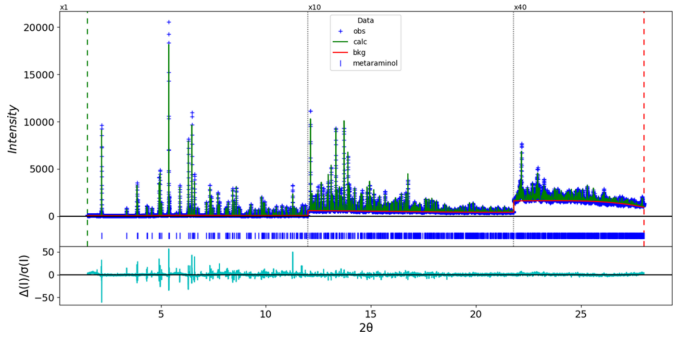

Figure 6
The Rietveld plot for (**I**). The blue crosses represent the observed data points, and the green line is the calculated pattern. The cyan curve is the normalized error plot, and the red line is the background curve. The blue tick marks indicate the peak positions. The vertical scale has been multiplied by a factor of 10× for $2\theta > 12.0°$, and by a factor of 40× for $2\theta > 21.8°$.

mental cell) and population analysis were carried out using *CRYSTAL23* (Erba *et al.*, 2023). The basis sets for the H, C, N and O atoms in the calculation were those of Gatti *et al.* (1994). The calculations were run on a 3.5 GHz PC using 8 *k*-points and the B3LYP functional, and took ∼1.9 h. The powder pattern of (**I**) has been submitted to ICDD for inclusion in the Powder Diffraction File.>

Acknowledgements

Use of the Advanced Photon Source at Argonne National Laboratory was supported by the U. S. Department of Energy, Office of Science, Office of Basic Energy Sciences, under Contract No. DE-AC02–06CH11357. We thank Saul Lapidus for his assistance in the data collection. We also thank the ICDD team – Megan Rost, Steve Trimble, and Dave Bohnenberger – for their contribution to research, sample preparation, and in-house XRD data collection and verification.

Funding information

Funding for this research was provided by: International Centre for Diffraction Data (grant No. 09-03).

References

Altomare, A., Cuocci, C., Giacovazzo, C., Moliterni, A., Rizzi, R., Corriero, N. & Falcicchio, A. (2013). *J. Appl. Cryst.* **46**, 1231–1235.
Antao, S. M., Hassan, I., Wang, J., Lee, P. L. & Toby, B. H. (2008). *Can. Mineral.* **46**, 1501–1509.
Bravais, A. (1866). *Etudes Cristallographiques.* Paris: Gauthier Villars.
Brenna, D., Marchesi, A. & Mihali, V. (2018). *Process for the preparation of metaraminol.* United States Patent US 10,087,136 B2.
Bruno, I. J., Cole, J. C., Kessler, M., Luo, J., Motherwell, W. D. S., Purkis, L. H., Smith, B. R., Taylor, R., Cooper, R. I., Harris, S. E. & Orpen, A. G. (2004). *J. Chem. Inf. Comput. Sci.* **44**, 2133–2144.
Crystal Impact. (2025). *DIAMOND*. Crystal Impact GbR, Bonn, Germany.
Dassault Systèmes. (2025). *BIOVIA Materials Studio 2025*. BIOVIA, San Diego, CA, USA.
David, W. I. F., Shankland, K., van de Streek, J., Pidcock, E., Motherwell, W. D. S. & Cole, J. C. (2006). *J. Appl. Cryst.* **39**, 910–915.
Donnay, J. D. H. & Harker, D. (1937). *Am. Mineral.* **22**, 446–467.
Erba, A., Desmarais, J. K., Casassa, S., Civalleri, B., Donà, L., Bush, I. J., Searle, B., Maschio, L., Edith-Daga, L., Cossard, A., Ribaldone, C., Ascrizzi, E., Marana, N. L., Flament, J.-P. & Kirtman, B. (2023). *J. Chem. Theory Comput.* **19**, 6891–6932.
Favre-Nicolin, V. & Černý, R. (2002). *J. Appl. Cryst.* **35**, 734–743.
Friedel, G. (1907). *Bull. Soc. Française Minéral.* **30**, 326–455.
Gatti, C., Saunders, V. R. & Roetti, C. (1994). *J. Chem. Phys.* **101**, 10686–10696.
Grauslyte, L., Bolding, N., Phull, M. & Jovaisa, T. (2022). *J. Crit. Care Med.* **8**, 195–203.
Groom, C. R., Bruno, I. J., Lightfoot, M. P. & Ward, S. C. (2016). *Acta Cryst.* B**72**, 171–179.
Kabekkodu, S., Dosen, A. & Blanton, T. N. (2024). *Powder Diffr.* **39**, 47–59.
Kaduk, J. A., Crowder, C. E., Zhong, K., Fawcett, T. G. & Suchomel, M. R. (2014). *Powder Diffr.* **29**, 269–273.
Kaduk, J. A., Dosen, A. & Blanton, T. N. (2026). In preparation.
Kim, S., Chen, J., Cheng, T., Gindulyte, A., He, J., He, S., Li, Q., Shoemaker, B. A., Thiessen, P. A., Yu, B., Zaslavsky, L., Zhang, J. & Bolton, E. E. (2023). *Nucleic Acids Res.* **51**, D1373–D1380.
Kresse, G. & Furthmüller, J. (1996). *Comput. Mater. Sci.* **6**, 15–50.
Lee, P. L., Shu, D., Ramanathan, M., Preissner, C., Wang, J., Beno, M. A., Von Dreele, R. B., Ribaud, L., Kurtz, C., Antao, S. M., Jiao, X. & Toby, B. H. (2008). *J. Synchrotron Rad.* **15**, 427–432.
Macrae, C. F., Sovago, I., Cottrell, S. J., Galek, P. T. A., McCabe, P., Pidcock, E., Platings, M., Shields, G. P., Stevens, J. S., Towler, M. & Wood, P. A. (2020). *J. Appl. Cryst.* **53**, 226–235.
Materials Design. (2024). *MedeA*. Materials Design Inc., San Diego, USA.
MDI (2025). *JADE Pro*. Materials Data, Livermore CA, USA.
O'Boyle, N. M., Banck, M., James, C. A., Morley, C., Vandermeersch, T. & Hutchison, G. R. (2011). *J. Cheminform.* **3**, 33.
Pu, Y., Zhu, Y. & Xiang, D. (2013). Synthesis method of metaraminol bitartrate. Chinese Patent CN103739504A.
Rammohan, A. & Kaduk, J. A. (2018). *Acta Cryst.* B**74**, 239–252.
Spackman, P. R., Turner, M. J., McKinnon, J. J., Wolff, S. K., Grimwood, D. J., Jayatilaka, D. & Spackman, M. A. (2021). *J. Appl. Cryst.* **54**, 1006–1011.
Sykes, R. A., McCabe, P., Allen, F. H., Battle, G. M., Bruno, I. J. & Wood, P. A. (2011). *J. Appl. Cryst.* **44**, 882–886.
Toby, B. H. & Von Dreele, R. B. (2013). *J. Appl. Cryst.* **46**, 544–549.
van de Streek, J. & Neumann, M. A. (2014). *Acta Cryst.* B**70**, 1020–1032.
Wang, J., Toby, B. H., Lee, P. L., Ribaud, L., Antao, S. M., Kurtz, C., Ramanathan, M., Von Dreele, R. B. & Beno, M. A. (2008). *Rev. Sci. Instrum.* **79**, 085105.
Wavefunction (2025). *Spartan '24.* Wavefunction Inc., Irvine, USA.
Wheatley, A. M. & Kaduk, J. A. (2019). *Powder Diffr.* **34**, 35–43.

supporting information

Acta Cryst. (2026). E**82** [https://doi.org/10.1107/S2056989026009497]

Structure of metaraminol hydrogen tartrate from synchrotron X-ray data and density functional theory calculations

Jacob K. Salazar, James A Kaduk, Anja Dosen and Thomas N. Blanton

Computing details

3-[(1*R*,2*S*)-2-Azaniumyl-1-hydroxypropyl]phenol (2*S*,3*S*)-hydrogen 2,3-dihydroxybutanedioate (I)

Crystal data

$C_9H_{14}NO_2^+ \cdot C_4H_5O_6^-$
M_r = 317.29
Orthorhombic, $P2_12_12_1$
a = 7.190512 (12) Å
b = 8.421634 (17) Å
c = 24.69323 (5) Å
V = 1495.32 (1) Å^3
Z = 4
D_x = 1.409 Mg m^{-3}
Synchrotron radiation, λ = 0.46873 Å
μ = 0.001 mm^{-1}
T = 295 K
cylinder, 2.0 × 1.5 mm

Data collection

11-BM, APS diffractometer
Specimen mounting: Kapton capillary
Data collection mode: transmission
Scan method: step
$2\theta_{min}$ = 0.510°, $2\theta_{max}$ = 49.995°, $2\theta_{step}$ = 0.001°

Refinement

Least-squares matrix: full
R_p = 0.090
R_{wp} = 0.105
R_{exp} = 0.039
$R(F^2)$ = 0.09024
49486 data points
Profile function: Finger-Cox-Jephcoat function parameters U, V, W, X, Y, SH/L: peak variance(Gauss) = Utan(Th)^2+Vtan(Th)+W: peak HW(Lorentz) = X/cos(Th)+Ytan(Th); SH/L = S/L+H/L U, V, W in (centideg)^2, X & Y in centideg 1.163, -0.126, 0.063, 0.000, 0.000, 0.002,
85 parameters
50 restraints
19 constraints
Weighting scheme based on measured s.u.'s
$(\Delta/\sigma)_{max}$ = 2.873
Background function: Background function: "chebyschev-1" function with 6 terms: 44.39(10), -9.67(15), -6.44(12), -0.91(18), 1.31(17), -5.45(13), Background peak parameters: pos, int, sig, gam: 5.974(12), 1.053(24)e4, 1.09(3)e4, 0.100,
Preferred orientation correction: Simple spherical harmonic correction Order = 2 Coefficients: 0:0:C(2,0) = -0.0120; 0:0:C(2,2) = 0.0660

Fractional atomic coordinates and isotropic or equivalent isotropic displacement parameters (Å^2)

	x	*y*	*z*	U_{iso}*/U_{eq}
O1	0.3342 (4)	0.8022 (3)	0.93215 (10)	0.0479 (6)*
O2	0.3359 (4)	0.5307 (3)	1.10736 (10)	0.0445 (5)*
N3	0.4468 (4)	0.6614 (4)	0.82720 (13)	0.0479 (6)*

C4	0.2734 (5)	0.6488 (4)	0.91486 (13)	0.0479 (6)*
C5	0.4270 (5)	0.5755 (4)	0.87984 (13)	0.0479 (6)*
C6	0.2282 (5)	0.5511 (4)	0.96343 (12)	0.0445 (5)*
C7	0.6176 (5)	0.5688 (5)	0.90906 (15)	0.0479 (6)*
C8	0.3051 (6)	0.5873 (4)	1.01338 (14)	0.0445 (5)*
C9	0.1121 (5)	0.4235 (4)	0.95835 (13)	0.0445 (5)*
C10	0.2652 (5)	0.4938 (4)	1.05747 (11)	0.0445 (5)*
C11	0.0749 (5)	0.3274 (4)	1.00251 (17)	0.0445 (5)*
C12	0.1529 (6)	0.3636 (4)	1.05258 (13)	0.0445 (5)*
H13	0.14930	0.66750	0.89080	0.0665*
H14	0.38411	0.45668	0.86620	0.0665*
H15	0.60500	0.49580	0.94340	0.0665*
H16	0.70849	0.49856	0.88244	0.0665*
H17	0.67350	0.67480	0.91330	0.0665*
H18	0.40460	0.68710	1.01580	0.0655*
H19	0.04630	0.38770	0.92000	0.0655*
H20	0.34520	0.74740	0.82580	0.0665*
H21	0.43010	0.59330	0.79430	0.0665*
H22	0.24880	0.87450	0.92230	0.0665*
H23	−0.02730	0.22950	1.00070	0.0655*
H24	0.11220	0.29700	1.08940	0.0655*
H25	0.25770	0.60010	1.12710	0.0655*
O26	0.5203 (4)	1.2468 (3)	0.80511 (12)	0.0480 (4)*
O27	0.5292 (3)	0.9921 (3)	0.83009 (11)	0.0480 (4)*
O28	−0.1329 (3)	1.0797 (3)	0.73408 (11)	0.0480 (4)*
O30	0.1607 (4)	0.9700 (3)	0.83668 (10)	0.0480 (4)*
O31	0.2265 (3)	1.0825 (3)	0.72509 (10)	0.0480 (4)*
C32	0.2339 (5)	1.1202 (4)	0.82380 (14)	0.0480 (4)*
C33	0.4494 (4)	1.1141 (4)	0.82050 (19)	0.0480 (4)*
C34	0.1555 (5)	1.1747 (4)	0.76783 (14)	0.0480 (4)*
C35	−0.0592 (4)	1.1695 (5)	0.76762 (16)	0.0480 (4)*
H36	0.18320	0.97650	0.72600	0.0675*
H37	0.22630	0.92780	0.86820	0.0675*
H38	0.19420	1.30100	0.76540	0.0675*
H39	0.19860	1.21030	0.85250	0.0675*
O29	−0.1365 (4)	1.2557 (3)	0.80333 (12)	0.0480 (4)*
H40	0.57713	0.71760	0.82517	0.0665*
H41	−0.26740	1.25380	0.80370	0.0675*

Geometric parameters (Å, º)

O1—C4	1.429 (3)	H15—C7	1.052 (4)
O1—H22	0.898 (3)	H16—C7	1.100 (4)
O2—C10	1.369 (3)	H17—C7	0.984 (4)
O2—H25	0.946 (3)	H18—C8	1.106 (3)
N3—C5	1.494 (3)	H19—C9	1.101 (3)
N3—H20	1.029 (3)	H20—N3	1.029 (3)
N3—H21	1.002 (3)	H21—N3	1.002 (3)

N3—H40	1.051 (3)	H22—O1	0.898 (3)
C4—O1	1.429 (3)	H23—C11	1.106 (3)
C4—C5	1.533 (3)	H24—C12	1.108 (3)
C4—C6	1.491 (3)	H25—O2	0.946 (3)
C4—H13	1.083 (3)	O26—C33	1.286 (3)
C5—N3	1.494 (3)	O27—C33	1.200 (3)
C5—C4	1.533 (3)	O28—C35	1.241 (3)
C5—C7	1.550 (4)	O30—C32	1.407 (3)
C5—H14	1.100 (3)	O30—H37	0.977 (3)
C6—C4	1.491 (3)	O31—C34	1.406 (3)
C6—C8	1.386 (3)	O31—H36	0.946 (3)
C6—C9	1.366 (3)	C32—O30	1.407 (3)
C7—C5	1.550 (4)	C32—C33	1.553 (3)
C7—H15	1.052 (4)	C32—C34	1.562 (4)
C7—H16	1.100 (4)	C32—H39	1.069 (3)
C7—H17	0.984 (4)	C33—O26	1.286 (3)
C8—C6	1.386 (3)	C33—O27	1.200 (3)
C8—C10	1.374 (3)	C33—C32	1.553 (3)
C8—H18	1.106 (3)	C34—O31	1.406 (3)
C9—C6	1.366 (3)	C34—C32	1.562 (4)
C9—C11	1.384 (3)	C34—C35	1.544 (3)
C9—H19	1.101 (3)	C34—H38	1.101 (4)
C10—O2	1.369 (3)	C35—O28	1.241 (3)
C10—C8	1.374 (3)	C35—C34	1.544 (3)
C10—C12	1.367 (3)	C35—O29	1.270 (3)
C11—C9	1.384 (3)	H36—O31	0.946 (3)
C11—C12	1.391 (3)	H37—O30	0.977 (3)
C11—H23	1.106 (3)	H38—C34	1.101 (4)
C12—C10	1.367 (3)	H39—C32	1.069 (3)
C12—C11	1.391 (3)	O29—C35	1.270 (3)
C12—H24	1.108 (3)	O29—H41	0.942 (3)
H13—C4	1.083 (3)	H40—N3	1.051 (3)
H14—C5	1.100 (3)	H41—O29	0.942 (3)

C4—O1—H22	108.8 (3)	C6—C9—H19	123.8 (3)
C10—O2—H25	112.5 (3)	C11—C9—H19	115.8 (3)
C5—N3—H20	107.6 (3)	O2—C10—C8	120.4 (3)
C5—N3—H21	114.6 (3)	O2—C10—C12	118.8 (3)
H20—N3—H21	106.9 (3)	C8—C10—C12	120.85 (19)
C5—N3—H40	110.1 (3)	C9—C11—C12	119.6 (2)
H20—N3—H40	108.3 (3)	C9—C11—H23	122.2 (4)
H21—N3—H40	109.0 (3)	C12—C11—H23	117.8 (4)
O1—C4—C5	108.2 (3)	C10—C12—C11	119.5 (2)
O1—C4—C6	109.0 (3)	C10—C12—H24	119.3 (3)
C5—C4—C6	112.9 (3)	C11—C12—H24	120.8 (4)
O1—C4—H13	106.5 (3)	C32—O30—H37	109.1 (3)
C5—C4—H13	110.1 (3)	C34—O31—H36	112.6 (3)
C6—C4—H13	110.0 (3)	O30—C32—C33	110.8 (3)

N3—C5—C4	111.4 (3)	O30—C32—C34	109.3 (3)
N3—C5—C7	109.8 (3)	C33—C32—C34	108.9 (3)
C4—C5—C7	112.9 (3)	O30—C32—H39	113.6 (3)
N3—C5—H14	101.6 (3)	C33—C32—H39	107.2 (3)
C4—C5—H14	109.7 (3)	C34—C32—H39	107.0 (3)
C7—C5—H14	111.0 (3)	O26—C33—O27	127.8 (3)
C4—C6—C8	120.5 (3)	O26—C33—C32	112.5 (3)
C4—C6—C9	119.6 (3)	O27—C33—C32	119.7 (3)
C8—C6—C9	119.89 (19)	O31—C34—C32	111.8 (3)
C5—C7—H15	108.7 (3)	O31—C34—C35	110.2 (3)
C5—C7—H16	105.5 (3)	C32—C34—C35	110.8 (3)
H15—C7—H16	102.6 (3)	O31—C34—H38	113.6 (3)
C5—C7—H17	112.2 (4)	C32—C34—H38	103.9 (3)
H15—C7—H17	118.7 (4)	C35—C34—H38	106.3 (3)
H16—C7—H17	108.0 (3)	O28—C35—C34	116.5 (3)
C6—C8—C10	119.74 (17)	O28—C35—O29	128.7 (3)
C6—C8—H18	118.3 (3)	C34—C35—O29	114.8 (3)
C10—C8—H18	121.9 (3)	C35—O29—H41	115.8 (3)
C6—C9—C11	120.4 (2)		

(I_VASP)

Crystal data

$C_9H_{14}NO_2^+ \cdot C_4H_5O_6^-$
M_r = 317.29
Orthorhombic, $P2_12_12_1$
a = 7.18988 Å
b = 8.42062 Å
c = 24.69000 Å
V = 1494.81 Å^3
Z = 4

Data collection

$h = \rightarrow$
$k = \rightarrow$
$l = \rightarrow$

Fractional atomic coordinates and isotropic or equivalent isotropic displacement parameters (Å²)

	x	y	z	B_{iso}*/B_{eq}
O1	0.19904	0.79641	0.90895	
O2	0.30367	0.55312	1.09380	
N3	0.43993	0.67441	0.82696	
C4	0.20728	0.62634	0.89994	
C5	0.40094	0.58234	0.87743	
C6	0.16477	0.53659	0.95149	
C7	0.56541	0.59839	0.91583	
C8	0.24506	0.58658	1.00022	
C9	0.04789	0.40382	0.95093	
C10	0.21364	0.50247	1.04809	
C11	0.01340	0.32210	0.99913	
C12	0.09585	0.36959	1.04753	
H13	0.10443	0.59411	0.86857	
H14	0.39033	0.45783	0.86419	

H15	0.55482	0.51329	0.94926
H16	0.69532	0.57332	0.89398
H17	0.57543	0.71824	0.93284
H18	0.33191	0.69278	1.00118
H19	−0.01707	0.36538	0.91312
H20	0.45057	0.79766	0.83301
H21	0.33607	0.65249	0.79796
H22	0.06961	0.82381	0.91785
H23	−0.07979	0.22003	0.99895
H24	0.07184	0.30291	1.08469
H25	0.23133	0.51970	1.12653
H40	0.56803	0.63905	0.81033
O26	0.52321	1.25511	0.80787
O27	0.53712	0.99571	0.83047
O28	−0.14693	1.09119	0.73653
O30	0.16346	0.95661	0.81546
O31	0.21301	1.10837	0.71535
C32	0.23428	1.11268	0.81422
C33	0.44886	1.11891	0.81698
C34	0.15305	1.18926	0.76289
C35	−0.05925	1.18289	0.76641
H36	0.15446	1.00232	0.71438
H37	0.18695	0.90728	0.85137
H38	0.19793	1.31362	0.75953
H39	0.18481	1.18368	0.84927
O29	−0.13548	1.27646	0.80279
H41	−0.29187	0125805	0.80531

Hydrogen-bond geometry (Å, º)

D—H···*A*	*D*—H	H···*A*	*D*···*A*	*D*—H···*A*
O29—H41···O26^{i}	1.14	1.33	2.464	173
O30—H37···O1	0.99	1.70	2.686	169
O31—H36···O29^{ii}	0.99	1.95	2.885	156
O31—H36···O28	0.99	2.36	2.644	96
N3—H40···O31^{iii}	1.05	1.72	2.762	172
N3—H21···O28^{ii}	1.05	1.69	2.718	166
N3—H20···O27	1.05	1.78	2.796	161
N3—H20···O30	1.05	2.50	3.111	116
O2—H25···O27^{iv}	1.00	1.76	2.709	157
O1—H22···O2^{iv}	0.98	2.19	3.113	155
C5—H14···O26	1.10	2.40	3.364	145
C12—H24···O26	1.09	2.72	3.758	154
C4—H13···O28	1.11	2.61	3.410	128
C9—H19···O29	1.09	2.95	4.033	171

Symmetry codes: (i) *x*−1, *y*, *z*; (ii) −*x*, *y*−1/2, −*z*+3/2; (iii) −*x*+1, *y*+1/2, −*z*+3/2; (iv) *x*−1/2, −*y*+3/2, −*z*+2.